Imaging with spatio-temporal modelling to characterize the dynamics of plant-pathogen lesions

Melen Leclerc*[1], Stéphane Jumel[1], Frédéric M. Hamelin[1], Rémi Treilhaud[1], Nicolas Parisey[1], and Youcef Mammeri[2]

[1]IGEPP, INRAE, Institut Agro, Rennes 1 University, Rennes, France

[2]ICJ, CNRS, Jean Monnet University, Saint-Etienne, France

* Corresponding author

email addresses :
melen.leclerc@inrae.fr, stephane.jumel@inrae.fr, frederic.hamelin@agrocampus-ouest.fr, rtreilhaud@live.fr, nicolas.parisey@inrae.fr, youcef.mammeri@math.cnrs.fr

Abstract

Within-host spread of pathogens is an important process for the study of plant-pathogen interactions. However, the development of plant-pathogen lesions remains practically difficult to characterize beyond the common traits such as lesion area. Here, we address this question by combining image-based phenotyping with mathematical modelling.

We consider the spread of *Peyronellaea pinodes* on pea stipules that were monitored daily with visible imaging. We assume that pathogen propagation on host-tissues can be described by the Fisher-KPP model where lesion spread depends on both a logistic growth and an homogeneous diffusion. Model parameters are estimated using a variational data assimilation approach on sets of registered images.

This modelling framework is used to compare the spread of an aggressive isolate on two pea cultivars with contrasted levels of partial resistance. We show that the expected slower spread on the most resistant cultivar is actually due to a decrease of diffusion and, to a lesser extent, growth rate.

These results demonstrate that spatial models with imaging allows one to disentangle the processes involved in host-pathogen interactions. Hence, promoting model-based phenotyping of interactions would allow a better identification of quantitative traits thereafter used in genetics and ecological studies.

keywords: ascochyta blight of pea, disease phenotyping, quantitative host resistance, computer vision, reaction-diffusion model, variational optimization

1 Introduction

Assessing life-history traits of pathogen on host plants is central to understand the adaptation of pathogens to plant resistance and to determine quantitative trait loci for both host resistance and pathogen aggressiveness [25]. The quantitative traits of host-pathogen interaction the most frequently measured are incubation and latency periods, spore production and lesion size [39]. In practice, they are often obtained after inoculating host, monitoring the development of the lesions caused by the pathogen and finally estimating the traits of interest. However, phenotyping the dynamics of host-pathogen interactions remains challenging and is often performed through inaccurate traits that, though they already contrast phenotypes, poorly describe the processes and can hide or skew

differences between individuals [26]. The lesion size is a good example to illustrate this as there are an infinity of spatial dynamics than can produce identical size at a given time. Considering the lesion growth rate is more informative but again, it ignores lesions shapes and depends on processes such as the local growth and the diffusion. Mechanistic models offer a mean to decipher the processes involved in host-pathogen interactions but are still seldom considered for analyzing plant disease phenotypic data [28, 26]. In this case the model should remain parsimonious enough so that the parameters can be identified from the data.

The recent development of image-based phenotyping methods enables *in vivo* non-destructive longitudinal monitoring of infected tissues. Besides allowing precise and automated quantification of necrotic plant tissues, that already improved disease phenotyping [e.g 23, 8, 51], imaging opens new possibilities to further investigate the spatial dimension of host-pathogen interactions. As illustrated by works on the development of human lesions, imaging data can be particularly interesting for fitting spatially explicit process-based models [21, 33]. It provides new insights into the main mechanisms involved in lesion development in relation with host immunity but also modelling tools for phenotyping. Perhaps surprisingly, although the main physiological mechanisms of plants and their parasites have been described by mathematical models [e.g 6, 47] the spread of lesions has received little attention by modellers [41, 31, 19, 26] and rarely validated against images [4].

In this study we consider the fungal pathogen *Peyronellaea pinodes* (formerly *Mycosphaerella pinodes and Didymella pinodes*) on pea as an example pathosystem to analyze its spread using modelling and imaging. With the two fungi *Phoma medicaginis* and *Ascochyta pisi*, *P. pinodes* belongs to the Ascochyta blight of pea disease complex that causes substantial yield losses worldwide [10]. In Europe, *P. pinodes* is generally the predominant and the most destructive species, though *P. medicaginis* is also prevalent and tends to develop later in the growing season [13, 14]. *P. pinodes* is able to infect all aerial parts of its host plant and induces necrotic growing lesions. The development of resistant cultivars to *P. pinodes* has been central for the integrated management of this disease, but difficult as only quantitative (or partial) resistance was available [42, 10]. For most fungal pathogens, quantitative host resistance alters spore production and infection as well as within-host growth [39, 25, 26]. The evaluation of quantitative host resistance on pathogen life-history traits is often performed in controlled conditions with *ad hoc* protocols. In the case of *P.*

pinodes partial resistance of pea can be assessed on inoculated detached leaflets, or stipules, by measuring necrotic lesions either manually [36] or with imaging [13].

We begin by presenting the experiment, including the image acquisition protocol and the processing framework, that allowed the longitudinal monitoring of lesions on inoculated pea stipules. Then, we consider the Fisher-KPP reaction-diffusion model to describe the spread of necrotic lesions on host tissues which is fitted to image sequences. We show that combining imaging and spatially explicit models enables a finer description of within-host spread of pathogen, including lesions coalescence, and allows one to disentangle local growth and diffusion of the necrosis. The comparison of estimated parameters obtained on two cultivars provides new insights into the effects of host quantitative resistance on lesion spread. We finish by discussing our work and how further developments inspired from biomedical research may contribute to improve our understanding of host-pathogen interactions and provide mathematical tools for precision phenotyping.

2 Materials and methods

2.1 Host inoculation experiment

The aggressive isolate of *P. pinodes* named *Mp 91.31.12* was inoculated on two pea cultivars previously tested in our laboratory: Solara, a common susceptible reference, and James, that reduces symptom development in controlled conditions [36]. These two cultivars are semi-leafless without conventional leaves but extended pairs of hypertrophied stipules below each stem node. For each cultivar, leaf stipules were inoculated according to a standard biotest protocol developed in our laboratory [36, 13]. Plants were grown in a climate chamber, kept at 18°C and with a 12h photoperiod, in 9cm diameter pots containing vermiculite and five pea seeds. When they reached the 6 leaf stage, stipules from nodes 3 and 4 were sampled and placed on tap water in a compartmented square Petri dish. The inoculum consisted in a pycnidiospore suspension whose concentration was determined with a haemocytometer and adjusted at 5×10^4 spores ml^{-1} following Onfroy et al. [36] protocol. For both cultivar, 16 pairs of attached stipules were inoculated by placing a 10μl droplet at their center. Afterwards, the Petri dishes containing the inoculated stipules were placed into transparent plastic containers to avoid drop evaporation and incubated in a

climatic chamber kept at 20°C and with a 14 h photoperiod. The protocol is summarized into a schematic diagram given in appendix (Fig. S1).

2.2 Image acquisition

The spread of lesions caused by the pathogen was assessed daily from 3 to 7 days after inoculation (Fig.1) following a standardized acquisition protocol developed for plant disease phenotyping [8, 13, 9]. Image acquisition was performed using two FotoQuantum LightPro 50 × 70 cm soft boxes, placed on both sides of the Petri dish with four daylight bulbs each (5400 K, 30 W). Pictures were taken with a Nikon D5300 digital camera equipped with an AF-S DX Micro Nikkor 40 mm 1:2.8G lens, on a Kaiser Repro stand, and with computer control using DigiCamControl software ver. 2.1.1.0. Aperture was set at F22 for maximal depth of field, iso 125, daylight white balance. Initial pictures were saved as RGB images with a resolution of 6000 × 4000 pixels.

2.3 Image processing

As illustrated in Figure 1, several processing steps were required to enable model fitting to image sequences. First, stipules (i.e. our region of interest) were extracted from raw images using the Simple Interactive Object Extraction algorithm [17] (Fig.1a). Second, images were registered (i.e. aligned to each other) using the Coherent Point Drift method [35], assuming rigid transformations and the first image (3 days after inoculation) as the reference (Fig.1b). Third, images were segmented by classifying pixels in either healthy, symptomatic or background states. The prediction of each pixel-class was based on several non-linear image features that captured local image characteristics. In particular we computed features for colours (e.g. Gaussian blur), edges (e.g. Laplacian), and textures (e.g. Hessian) at different scales using spherical filters with radii varying from 1 to 16 pixels. Based on these features, Random Forest classifiers were trained for each date of observation using the Trainable Waikato Environment for Knowledge Analysis (Weka) [2]. They were tested on ground truth images from an independent study [13] and showed good performances to classify pixels (Table S1), and thus separate background, leaf and symptomatic areas. Afterwards, these classifiers were used to process the full dataset and to get three probability images giving the probabilities of each pixel to be in each state (e.g. Figs.1c & S2 for state symptomatic). Pixels classification is actually obtained

using a standard cutoff of 0.5 on each probability. To finish with, we considered the Jaccard index (i.e. the intersection over the union of the two sets, that can vary between 0 and 100%) as a measure of stipules deformation, that was computed for each date assuming the 3^{rd} day as the reference set. All the images and classifiers are available in an open dataverse [22, 27].

2.4 Spatial lesion growth model

Most existing models for the spread of plant pathogens within host tissues are rather spatially implicit and generally assume a constant radial growth rate and a simplified geometry of the host organ [41, 31, 19]. Yet, these models were able to fit non-spatial lesion size data [26], including for the particular *P. pinodes*-pea pathosystem [13].

Here, we consider the Fisher-KPP equation as a model for the spatio-temporal dynamics of lesions. Because pathogen density cannot be directly inferred from common observations of symptoms in biotests, we describe the spread of the probability of infection, and thus the appearance of host tissues, rather than pathogen load. The Fisher-KPP equation was introduced in 1937 by Fisher [16] and Kolmogorov-Petrovsky-Piskunov [24] as a semilinear parabolic partial differential equation (PDE) combining Fick's diffusion with logistic growth. Let $\Omega \subset \mathbb{R}^2$ be the stipules area, the Fisher-KPP equation reads as the following reaction-diffusion equation, for the position $\mathbf{x} = (x, y) \in \Omega$ and the time $t > t_0$

$$\frac{\partial u}{\partial t}(\mathbf{x}, t) = D\Delta u(\mathbf{x}, t) + au(\mathbf{x}, t)\left(1 - u(\mathbf{x}, t)\right). \tag{1}$$

where $u(\mathbf{x}, t)$ the probability that the host is infected at location $\mathbf{x}$ and time t, $D > 0$ is the diffusion coefficient, $a \geq 0$ the growth rate. The initial conditions are given by an initial image u_0 as

$$u(\mathbf{x}, t = t_0) = u_0(\mathbf{x}) \text{ in } \Omega.$$

Assuming the pathogen cannot move out of the leaf, homogeneous Neumann boundary conditions are imposed

$$\frac{\partial u}{\partial n}(\mathbf{x}, t) = 0 \text{ on } \partial\Omega.$$

This model exhibits traveling waves with asymptotic speed $2\sqrt{aD}$ which is coherent with the assumption of a constant radial growth rate considered in

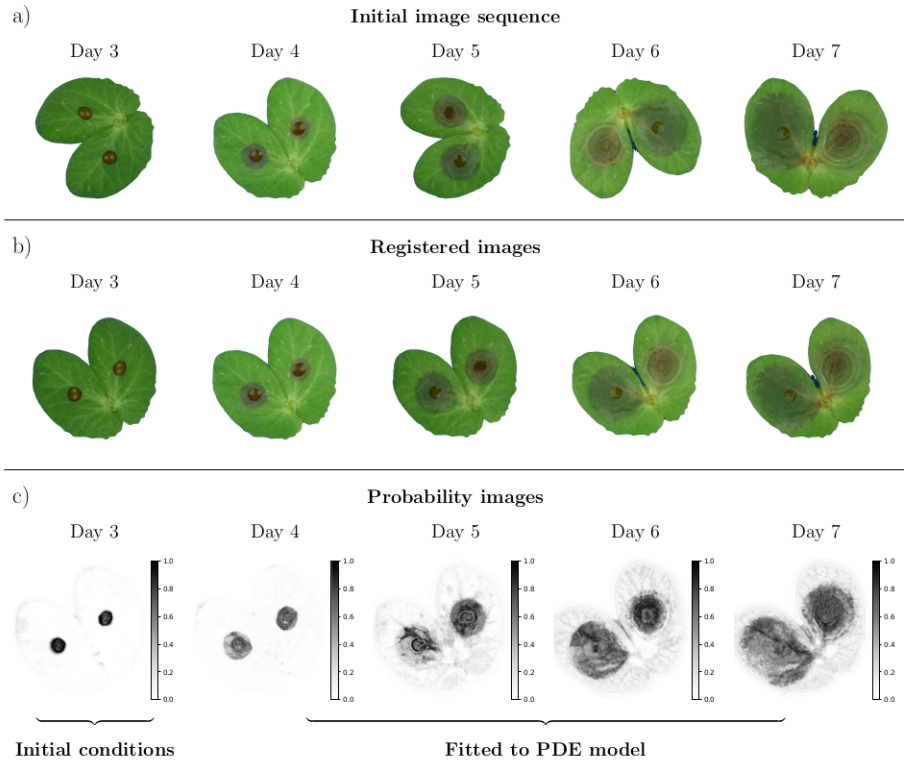

Figure 1: Schematic representation of lesion growth monitoring through imaging. The initial RGB images (a) are first registered to align stipules in time (b). Afterwards, a supervised segmentation is performed to produce probability maps indicating the probability of each pixel to be in either healthy, symptomatic or background classes. Probability images of the symptomatic state (c) are used for fitting the Fisher-KPP model. Images of day 3 are used as initial conditions while the remaining 4 images are used to estimate the pathogen local growth rate $\hat{a}$ and diffusion coefficient $\hat{D}$ that are actually two distinct life-history traits of within-host pathogen spread.

several studies and supported by non-spatial lesion data [26, 13].

Numerical solutions of the model are obtained by computing the spatial domain Ω with a level-set formalism so the boundaries $\partial\Omega$ match those of the leaves in the image [37, 48], and solving the partial differential equations using explicit Euler finite differences in time and second order centered finite differences in space. More details on these numerical aspects are provided in supplementary information 4.

2.5 Parameters estimation from image sequences

For each inoculated stipule, the observations consisted in a set of registered images $u_{reg}(\mathbf{x}, \mathbf{t})$ for times after inoculation $\mathbf{t} = \{t_3, t_4, t_5, t_6, t_7\}$ (Fig. 1). Parameters identification consisted in seeking estimates $\hat{\theta}$ such that the output of the spatial model $u(\mathbf{x}, t, \theta)$ matches these observations. Depending on the estimation problem, inverse problems or statistical inference of reaction-diffusion can be addressed by several methods such as mathematical analysis, maximum likelihood or non-linear least-squares [49]. When observations are image sequences it is more relevant to rely on data assimilation methods that have been developed and used to fit models in fluid dynamics [38] or biomedical modelling [33]. We consider a variational data assimilation approach based on optimal control theory [3]. The estimation procedure is based on the nonlinear least-squares cost function:

$$J(\theta) = \frac{1}{2} \sum_{t \in \mathbf{t}} \sum_{\mathbf{x} \in \Omega} (u(\mathbf{x}, t, \theta) - u_{reg}(\mathbf{x}, t))^2. \tag{2}$$

Following the variational assimilation framework [3], estimates $\hat{\theta}$ are found by minimizing $J(\theta)$ thanks to the Lagrangian function $\mathcal{L}(\theta)$ and a numerical procedure both detailed in appendix S4.2.

In our case there is no obvious link between the RGB images and the probability of infection u. To overcome this issue one can use appearance models, trained by experts, to predict interpretable data from the features of the raw images. In our case, we apply the supervised Random Forest classifiers to transform the color images into probability images (Fig. 1), thereafter considered as observations $u_{reg}(\mathbf{x}, \mathbf{t})$ in the cost function (2) for parameters estimation [21]. For each image sequence, the image of the 3^{rd} day provides the initial conditions ($t_0 = t_3$ and $u_0(\mathbf{x}) = u_{reg}(\mathbf{x}, t_3)$) while the remaining 4 images at times $\{t_4, t_5, t_6, t_7\}$ enables data assimilation and stable estimation of parameters [11].

As the diffusion coefficient depends on image size, we rather consider the relative diffusion, i.e. the raw diffusion coefficient divided by stipules area (S4.3). The model was fitted to the 2×16 inoculated stipules and we compared the two cultivars through one-way ANOVAs on the estimated diffusion coefficient $\hat{D}$ and growth rate $\hat{a}$. The adequacy of the Fisher-KPP model to the data was assessed visually by looking at the raw residuals for each date, i.e. $[u(\mathbf{x}, t_i, \hat{\theta}) - u_{reg}(\mathbf{x}, t_i)]$ for $t_i \in \mathbf{t}$.

3 Results

The Fisher-KPP model and its numerical resolution were able to describe the spread and the coalescence of lesions caused by *P. pinodes* on pea stipules as observed in standard biotests (Fig.2, Movies M1-2). The image processing framework associated with the data assimilation method allowed us to fit the reaction-diffusion model that captured the essential patterns of the spatio-temporal data. Overall, the visual assessment of raw residuals distributions points out a good centering with an increasing heteroscedasticity and a negative skewness with time (Figs. S4-5). This pattern might be partially explained by the change of the appearance of symptomatic and healthy tissues in time that become more difficult to separate for an annotator, and thus for an algorithm. Even if the trained Random Forest classifiers showed good performances to classify pixels with 0.5 thresholds, pixel classification became less certain over time with higher and lower probabilities in respectively healthy and symptomatic areas. Another explanation of the discrepancy between the model and the data is the change of stipules shape. Although stipules deformation remained limited with Jaccard indexes above 80 for all individuals (Fig.3), it may have induced some bias in the alignment of lesions and errors between the PDE model and images as illustrated in Figure 2b at day 7.

We successfully estimated the growth rate $\hat{a}$ and the diffusion coefficient $\hat{D}$ for the 32 monitored individuals (Table S3). James cultivar was characterized by smaller stipules than Solara with average surfaces of 4.49 and 7.93 cm^2 respectively. James cultivar had mean estimated growth rate $\hat{a}$ and diffusion coefficient $\hat{D}$ of respectively 0.496 and 0.291 against 0.536 and 0.489 for the more susceptible cultivar Solara. Analyses of variance pointed out significant differences between cultivars for both parameters (p-values < 0.05, Table S4), even if the gap between the distributions of estimates was higher for $\hat{D}$ (Fig.

4a) than for $\hat{a}$ (Fig. 4b). Such results suggest that, in our particular case, quantitative resistance reduced the propagation of the infection by decreasing the diffusion coefficient and, to a lesser extent the growth rate. Therefore, for inoculated stipules with identical areas and shapes, lesions caused by *P. pinodes* will spread at a higher speed, and thus coalesce and reach edges earlier, on Solara than on James.

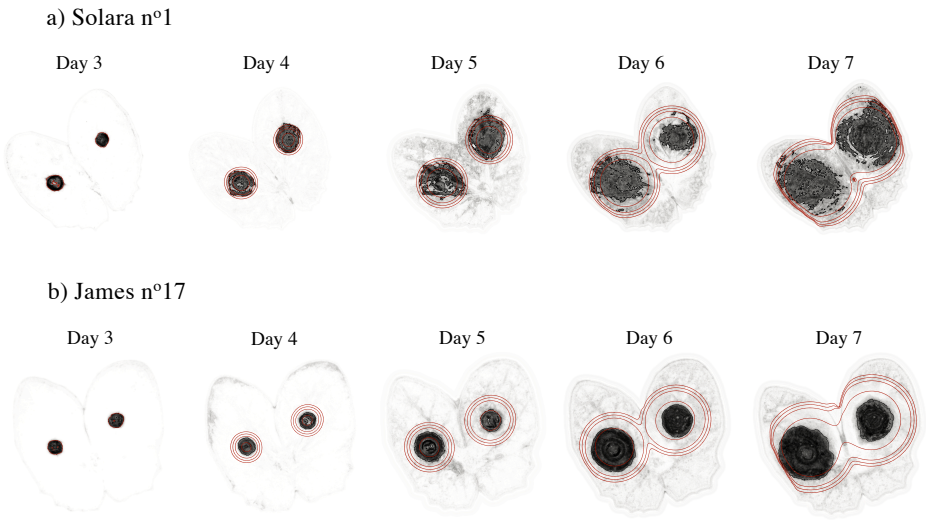

Figure 2: Visualization of model prediction against image data. The solution of the fitted Fisher-KPP equation, i.e. with optimal estimated parameters $\hat{\theta}$, is represented through time by contours $(0.2, 0.3, 0.4, 0.5)$ overlying the image sequences of the symptomatic class for example stipules of Solara (a) et James (b) cultivars. This comparison between the spatial model and the data is also available in two movies provided as supplementary materials (Movies S1-S2).

4 Discussion

In this study we combined image processing and mathematical modelling to investigate the dynamics of host-pathogen interactions. We showed that a longitudinal monitoring of inoculated leaves through visible imaging provides data to fit reaction-diffusion models that describe the spatio-temporal spread of pathogen on host tissues. While such methodological approaches are common in biomedical sciences [e.g 20, 33] they are original in plant pathology. Here,

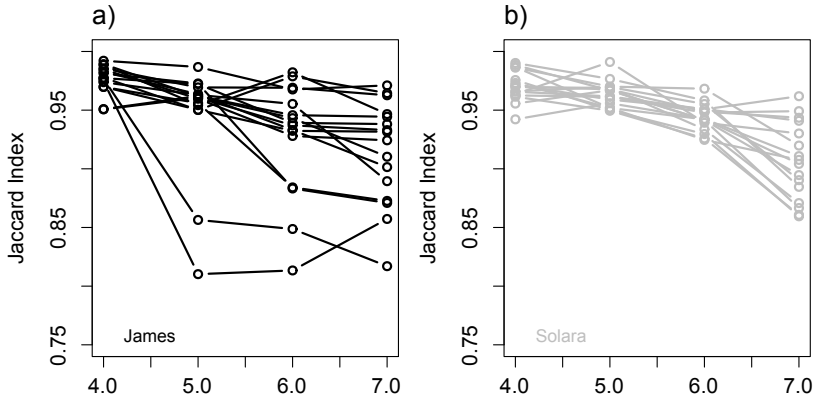

Figure 3: Visualization of stipules deformation in time. Change in the Jaccard index with time for cultivars James (a) and Solara (b). At each time after inoculation the Jaccard index was calculated in comparison with the image at day 3, also used as a reference for image registration.

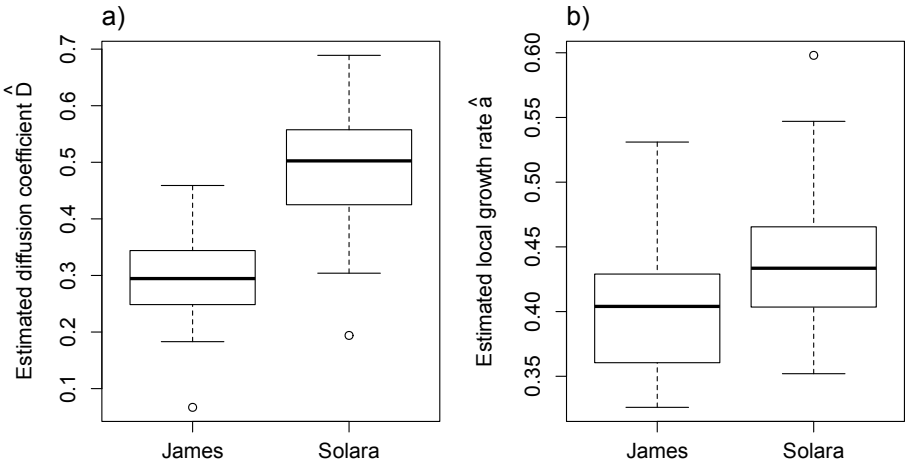

Figure 4: Distributions of the estimated parameters. a) diffusion coefficient $\hat{D}$ with a mean values of 0.291 for James against 0.489 for the more susceptible cultivar Solara, b) local growth rate $\hat{a}$ with mean values of 0.496 and 0.536 for respectively James and Solara. All estimated coefficient are available in supplementary information (Table S3).

we considered the fungal pathogen *P. pinodes* on pea as an example pathosystem and used the Fisher-KPP equation to model necrotrophic lesions. Using this PDE model with a variational data assimilation method we were able to capture the essential patterns of image-sequences data and disentangle growth and diffusion. These processes are actually two distinct life-history traits that both explain host colonization by the pathogen through lesions. They provide a finer description of the interaction but cannot be determined without the use of spatially-explicit models with spatial information, as provided by images, as different growth rate and diffusion can lead to identical lesion speed. Furthermore, while lesions coalescence, different leaves sizes, or lesion saturation at leaves boundaries can be problematic when comparing lesion sizes in common aggressiveness biotests, the inference of parameters in parsimonious PDE models can handle properly such situations.

We assessed the development of an aggressive isolate on two cultivars with contrasted level of partial resistance using a standard protocol developed for screening both pathogen aggressiveness and host resistance [36]. Our results were consistent with previous findings as the spread of lesions caused by *P. pinodes* was slower on James than Solara. Most interestingly, in this particular case we demonstrated that quantitative host resistance decreased significantly infection diffusion and, to a lesser extent, its local growth rate. Of course, we cannot generalize these effects of plant resistance as they should be further confirmed on a larger panel of pathogen isolates and host genotypes. Yet, these results show how combining advanced imaging methods and mechanistic models can help to improve the comparison of cultivars (or isolates) and gain new insights into plant resistance to disease. Although the detected effects of resistance may not be a posteriori surprising, they remain impossible to identify without the use of spatial models and data. Optical sensors recently percolated in plant sciences and contributed to recent development of precision phenotyping for plant diseases [30, 23, 51]. On the other side the usefulness of mechanistic models for analyzing phenotypic data is recognized [e.g. 28, 26] but remains seldom considered. We think that promoting the use of mechanistic models for processing precision phenotyping data would be particularly relevant for assessing the genetic architecture of traits, either for the plant or the pathogen, understanding pathogen adaptation to plant resistance and developing new cultivars.

Although our modelling framework was able to describe the visible spread of nectrotrophic lesions caused by *P. pinodes* and provided original knowledge on this pathosystem, it may be improved and extended on several points. Firstly,

for the sake of simplicity we ignored stipules deformation. This change in the shape of host organs caused by parasitism frequently occurs in plants and would be worth considering using existing mathematical and numerical methods for explicit modelling of shapes [37, 40] or plant growth [5]. While such improvement would increase the complexity of the model, it may contribute to decrease the discrepancy between the model and the data, and perhaps, help to identify genotypes that are less susceptible to disease-induced deformation. Secondly, the inoculated host leaves were digitalized through visible imaging and the reaction-diffusion model was fitted to probability images obtained with trained classifiers [21]. The appearance models, learned by experts, that transform raw image into an output which match with the state variable of the process model can have an influence on data assimilation. In our case we could improve the classifiers to reduce the noise that occur in time by training more advanced algorithm for pixel-based segmentation or include some filtering after predictions (e.g. morphological closing). Comparing different appearance models and assessing how they modify parameters estimation would be interesting, especially for pathosystems that cause unclear lesions that are difficult to annotate. Moreover, because there is no direct relationship between the appearance of symptoms and pathogen density in infected tissues we rather considered the spread of the probability of infection. Although this choice could be criticized it seems to describe well enough the dynamics of infections. In further studies it would be very interesting to assess the spread of pathogen density using destructive sampling with real-time quantitative PCR [29, 1] and non-destructive monitoring, e.g. with bioluminescence imaging [50]. Thirdly, as lesions caused by *P. pinodes* appeared to spread at a constant speed with quite homogeneous patterns we choose the Fisher-KPP equation. Albeit this first model already described the essential patterns of the data it would be interesting to relax some of its assumptions to improve the description of the observed spatial dynamics. For instance, one could consider a heterogeneous diffusion to capture the acceleration that seems to occur at the end of the experiment. Moreover, the Fisher-KPP equation won't be appropriate to describe the spreading processes that occur in all pathosystems. The spatial dynamics of plant-pathogen lesions remains poorly addressed and further works could benefit from theoretical knowledge on PDE for propagating systems and existing models for the spread of invasive organisms [32, 45], microbial populations and fungal colonies [6], or human lesions [21, 33]. For example, the effect of leaf veins that can guid lesion spread in some pathosystems could be considered through advection terms or

by considering hybrid reaction-diffusion models with different dynamics on host tissues (2D) and veins (1D) [45]. On the other side, like microbial populations in controlled media, plant-pathogen lesions can be an interesting experimental systems to test and feed some mathematical theories [34, 18]. Fourthly, our model ignored any host response to infection and further development could take into account some key physiological and immune processes. For instance it would be worth including ontogenetic and disease-induced changes in host susceptibility, e.g. caused by senescence or hypersensitive responses, that are known to occur in several pathosystems and can be spatially localized on leaf tissues [12, 43].

From an epidemiological point of view the within-host dynamics of the pathogen is an important phase that can have strong impact on epidemics at the population level. Scaling-up the behaviour of epidemics from individuals to populations is still a difficult question for mathematical and computational epidemiology and, at least in the case of plant diseases, the within-host spread of pathogens is either ignored or extremely simplified compared to other epidemiological processes such as spores production [46, 41, 19, 32]. This is mainly due to the challenges of multiscale and spatial modelling, but perhaps, also to the lack of spatial models for within-host pathogen development. Thus, we believe that besides providing new fundamental knowledge and phenotyping tools, spatial lesions models that describe observable spread of pathogen on host organs would also contribute to improve modelling works focused on higher scales. In addition, new insights into the effects of host resistance on within-host dynamics would also feed models for understanding the durability plant resistance to diseases [7, 15, 44]. For instance, the impact of partial resistance on either the diffusion coefficient or the local growth rate may affect differently pathogen fitness and have contrasted impacts on pathogen invasion, persistence and evolution.

5 Acknowledgements

This study was funded by the Bretagne Loire University and the Plant Health and Environment Division of INRAE through StartIRM and MODIM projects. We thank Alain Baranger, Christophe Le May, Agathe Dutt, Lydia Bousset and Tristan Boureau for useful discussions, and Claudine Pasco and Amélie Morin for their help during the experiment.

References

[1] C. Akimoto-Tomiyama, A. Furutani, and H. Ochiai. Real time live imaging of phytopathogenic bacteria xanthomonas campestris pv. campestris maff106712 in 'plant sweet home'. *PLoS One*, 9(4):e94386, 2014.

[2] I. Arganda-Carreras, V. Kaynig, C. Rueden, K. W. Eliceiri, J. Schindelin, A. Cardona, and H. Sebastian Seung. Trainable weka segmentation: a machine learning tool for microscopy pixel classification. *Bioinformatics*, 33(15):2424–2426, 2017.

[3] M. Asch, M. Bocquet, and M. Nodet. *Data assimilation: methods, algorithms, and applications*. SIAM, 2016.

[4] E. Belin, F. Chapeau-Blondeau, and D. Rousseau. Modèle stochastique et représentation par graphe pour le suivi spatio-temporel de pathogènes à la surface de feuilles par imagerie. In *25ème Colloque GRETSI sur le Traitement du Signal et des Images*, page 4, 2015.

[5] A. Bonneu, Y. Dumont, H. Rey, C. Jourdan, and T. Fourcaud. A minimal continuous model for simulating growth and development of plant root systems. *Plant and soil*, 354(1):211–227, 2012.

[6] G. P. Boswell, H. Jacobs, F. A. Davidson, G. M. Gadd, and K. Ritz. Growth and function of fungal mycelia in heterogeneous environments. *Bulletin of Mathematical Biology*, 65(3):447–477, 2003.

[7] R. Bourget, L. Chaumont, C.-E. Durel, and N. Sapoukhina. Sustainable deployment of qtls conferring quantitative resistance to crops: first lessons from a stochastic model. *New Phytologist*, 206(3):1163–1171, 2015.

[8] L. Bousset, M. Palerme, M. Leclerc, and N. Parisey. Automated image processing framework for analysis of the density of fruiting bodies of leptosphaeria maculans on oilseed rape stems. *Plant Pathology*, 68(9):1749–1760, 2019.

[9] L. Bousset, P. Vallée, R. Delourme, N. Parisey, M. Palerme, and M. Leclerc. Besides stem canker severity, oilseed rape host genotype matters for the production of Leptosphaeria maculans fruit bodies. *Fungal Ecology*, 52:101076, Aug. 2021. ISSN 1754-5048. doi: 10.1016/j.funeco.2021.

101076. URL https://www.sciencedirect.com/science/article/pii/S1754504821000386.

[10] T. Bretag, P. J. Keane, and T. Price. The epidemiology and control of ascochyta blight in field peas: a review. *Australian Journal of Agricultural Research*, 57(8):883–902, 2006.

[11] M. Cristofol and L. Roques. Stable estimation of two coefficients in a nonlinear fisher–kpp equation. *Inverse problems*, 29(9):095007, 2013.

[12] A. Dolatabadian, J. Batley, D. Edwards, and M. Barbetti. Virulence/avirulence patterns among leptosphaeria maculans isolates determines expression of resistance, senescence and yellowing in cotyledons of brassica napus. *European Journal of Plant Pathology*, 156(4):1077–1089, 2020.

[13] A. Dutt, D. Andrivon, S. Jumel, G. Le Roy, A. Baranger, M. Leclerc, and C. Le May. Life history traits and trade-offs between two species of the ascochyta blight disease complex of pea. *Plant Pathology*, 69(6):1108–1124, 2020.

[14] A. Dutt, R. Anthony, D. Andrivon, S. Jumel, G. Le Roy, A. Baranger, M. Leclerc, and C. Le May. Competition and facilitation among fungal plant parasites affect their life-history traits. *Oikos*, 130(4):652–667, 2021.

[15] F. Fabre, J.-B. Burie, A. Ducrot, S. Lion, Q. Richard, and R. Djidjou-Demasse. An epi-evolutionary model for predicting the adaptation of spore-producing pathogens to quantitative resistance in heterogeneous environments. *Evolutionary applications*, 15(1):95–110, 2022.

[16] R. Fisher. The wave of advance of an advantageous gene. *Annu. Eugenics*, 7(355-366), 1937.

[17] G. Friedland, K. Jantz, and R. Rojas. Siox: Simple interactive object extraction in still images. In *Seventh IEEE International Symposium on Multimedia (ISM'05)*, pages 7–pp. IEEE, 2005.

[18] S. R. Gandhi, E. A. Yurtsev, K. S. Korolev, and J. Gore. Range expansions transition from pulled to pushed waves as growth becomes more cooperative in an experimental microbial population. *Proceedings of the National Academy of Sciences*, 113(25):6922–6927, 2016.

[19] G. Garin, C. Fournier, B. Andrieu, V. Houlès, C. Robert, and C. Pradal. A modelling framework to simulate foliar fungal epidemics using functional–structural plant models. *Annals of botany*, 114(4):795–812, 2014.

[20] A. Habbal, H. Barelli, and G. Malandain. Assessing the ability of the 2d fisher–kpp equation to model cell-sheet wound closure. *Mathematical Biosciences*, 252:45–59, 2014.

[21] C. Hogea, C. Davatzikos, and G. Biros. An image-driven parameter estimation problem for a reaction–diffusion glioma growth model with mass effects. *Journal of mathematical biology*, 56(6):793–825, 2008.

[22] S. Jumel, A. Dutt, M. Leclerc, and N. Parisey. Segmentation of ascochyta blight symptoms on pea stipules, 2022. URL `https://doi.org/10.57745/5B1XGU`.

[23] P. Karisto, A. Hund, K. Yu, J. Anderegg, A. Walter, F. Mascher, B. A. McDonald, and A. Mikaberidze. Ranking quantitative resistance to septoria tritici blotch in elite wheat cultivars using automated image analysis. *Phytopathology*, 108(5):568–581, 2018.

[24] A. Kolmogorov, I. Petrovsky, and N. Piscounoiv. Etude de l'équation de la diffusion avec croissance de la quantité de la matière et son application à un problème biologique. *Bull. Univ. Moscow*, Ser. A 1:1–25, 1937.

[25] C. Lannou. Variation and selection of quantitative traits in plant pathogens. *Annual review of phytopathology*, 50:319–338, 2012.

[26] M. Leclerc, J. A. Clément, D. Andrivon, and F. M. Hamelin. Assessing the effects of quantitative host resistance on the life-history traits of sporulating parasites with growing lesions. *Proceedings of the Royal Society B*, 286 (1912):20191244, 2019.

[27] M. Leclerc, S. Jumel, F. Hamelin, R. Treilhaud, N. Parisey, and Y. Mammeri. Image sequences of growing lesions - Ascochyta blight of pea, 2022. URL `https://doi.org/10.57745/MQXKCP`.

[28] K. Leonard and C. Mundt. Methods for estimating epidemiological effects of quantitative resistance to plant diseases. *Theoretical and applied genetics*, 67(2):219–230, 1984.

[29] J. G. Maciá-Vicente, H.-B. Jansson, N. J. Talbot, and L. V. Lopez-Llorca. Real-time pcr quantification and live-cell imaging of endophytic colonization of barley (hordeum vulgare) roots by fusarium equiseti and pochonia chlamydosporia. *New phytologist*, 182(1):213–228, 2009.

[30] A.-K. Mahlein. Plant disease detection by imaging sensors–parallels and specific demands for precision agriculture and plant phenotyping. *Plant disease*, 100(2):241–251, 2016.

[31] Y. Mammeri, J. Burie, A. Calonnec, T. Cokelaer, E. Costes, M. Langlais, and C. Pradal. Modelling of the airborne dispersal of a pathogen over a structured vegetal cover. In *6th International Workshop on Functional-Structural Plant Models*, pages 55–57, 2010.

[32] Y. Mammeri, J. B. Burie, M. Langlais, and A. Calonnec. How changes in the dynamic of crop susceptibility and cultural practices can be used to better control the spread of a fungal pathogen at the plot scale? *Ecological modelling*, 290:178–191, 2014.

[33] A. Mang, S. Bakas, S. Subramanian, C. Davatzikos, and G. Biros. Integrated biophysical modeling and image analysis: application to neuro-oncology. *Annual review of biomedical engineering*, 22:309–341, 2020.

[34] M. J. Müller, B. I. Neugeboren, D. R. Nelson, and A. W. Murray. Genetic drift opposes mutualism during spatial population expansion. *Proceedings of the National Academy of Sciences*, 111(3):1037–1042, 2014.

[35] A. Myronenko and X. Song. Point set registration: Coherent point drift. *IEEE transactions on pattern analysis and machine intelligence*, 32(12): 2262–2275, 2010.

[36] C. Onfroy, A. Baranger, and B. Tivoli. Biotic factors affecting the expression of partial resistance in pea to ascochyta blight in a detached stipule assay. *European Journal of Plant Pathology*, 119(1):13–27, 2007.

[37] S. Osher and R. Fedkiw. *Level Set Methods and Dynamic Implicit Surfaces*. Springer New York, 2002.

[38] N. Papadakis and É. Mémin. Variational assimilation of fluid motion from image sequence. *SIAM Journal on Imaging Sciences*, 1(4):343–363, 2008.

[39] B. Pariaud, V. Ravigné, F. Halkett, H. Goyeau, J. Carlier, and C. Lannou. Aggressiveness and its role in the adaptation of plant pathogens. *Plant Pathology*, 58(3):409–424, 2009.

[40] I. Pineda and O. Gwun. Leaf modeling and growth process simulation using the level set method. *IEEE Access*, 5:15948–15959, 2017.

[41] J. A. Powell, I. Slapničar, and W. van der Werf. Epidemic spread of a lesion-forming plant pathogen—analysis of a mechanistic model with infinite age structure. *Linear Algebra and its Applications*, 398:117–140, 2005.

[42] S. Prioul, A. Frankewitz, G. Deniot, G. Morin, and A. Baranger. Mapping of quantitative trait loci for partial resistance to mycosphaerella pinodes in pea (pisum sativum l.), at the seedling and adult plant stages. *Theoretical and Applied Genetics*, 108(7):1322–1334, 2004.

[43] B. Richard, S. Jumel, F. Rouault, and B. Tivoli. Influence of plant stage and organ age on the receptivity of pisum sativum to mycosphaerella pinodes. *European Journal of Plant Pathology*, 132(3):367–379, 2012.

[44] L. Rimbaud, F. Fabre, J. Papaïx, B. Moury, C. Lannou, L. G. Barrett, and P. H. Thrall. Models of plant resistance deployment. *Annual Review of Phytopathology*, 59, 2021.

[45] L. Roques and O. Bonnefon. Modelling population dynamics in realistic landscapes with linear elements: A mechanistic-statistical reaction-diffusion approach. *PloS one*, 11(3):e0151217, 2016.

[46] J. Segarra, M. Jeger, and F. Van den Bosch. Epidemic dynamics and patterns of plant diseases. *Phytopathology*, 91(19):1001–1010, 2001.

[47] D. Sellier and Y. Mammeri. Diurnal dynamics of phloem loading: theoretical consequences for transport efficiency and flow characteristics. *Tree physiology*, 39(2):300–311, 2019.

[48] J. Sethian. *Level Set Methods and Fast Marching Methods: Evolving Interfaces in Computational Geometry, Fluid Mechanics, Computer Vision, and Materials Science*. Cambridge University Press, 1999.

[49] S. Soubeyrand and L. Roques. Parameter estimation for reaction-diffusion models of biological invasions. *Population ecology*, 56(2):427–434, 2014.

[50] X. Xu, S. A. Miller, F. Baysal-Gurel, K.-H. Gartemann, R. Eichenlaub, and G. Rajashekara. Bioluminescence imaging of clavibacter michiganensis subsp. michiganensis infection of tomato seeds and plants. *Applied and environmental microbiology*, 76(12):3978–3988, 2010.

[51] S. Yates, A. Mikaberidze, S. G. Krattinger, M. Abrouk, A. Hund, K. Yu, B. Studer, S. Fouche, L. Meile, D. Pereira, et al. Precision phenotyping reveals novel loci for quantitative resistance to septoria tritici blotch. *Plant phenomics*, 2019, 2019.